doi:10.1093/brain/awy320 BRAIN 2019: 142; 391–411 | 391

BRAIN
A JOURNAL OF NEUROLOGY

The role of astrocytes in seizure generation: insights from a novel *in vitro* seizure model based on mitochondrial dysfunction

Felix Chan,[1,2] Nichola Z. Lax,[2] Caroline Marie Voss,[3] Blanca Irene Aldana,[3] Shuna Whyte,[1] Alistair Jenkins,[4] Claire Nicholson,[4] Sophie Nichols,[1] Elizabeth Tilley,[1] Zoe Powell,[1] Helle S. Waagepetersen,[3] Ceri H. Davies,[5,†] Doug M. Turnbull[2] and Mark O. Cunningham[1,6]

Approximately one-quarter of patients with mitochondrial disease experience epilepsy. Their epilepsy is often severe and resistant towards conventional antiepileptic drugs. Despite the severity of this epilepsy, there are currently no animal models available to provide a mechanistic understanding of mitochondrial epilepsy. We conducted neuropathological studies on patients with mitochondrial epilepsy and found the involvement of the astrocytic compartment. As a proof of concept, we developed a novel brain slice model of mitochondrial epilepsy by the application of an astrocytic-specific aconitase inhibitor, fluorocitrate, concomitant with mitochondrial respiratory inhibitors, rotenone and potassium cyanide. The model was robust and exhibited both face and predictive validity. We then used the model to assess the role that astrocytes play in seizure generation and demonstrated the involvement of the GABA-glutamate-glutamine cycle. Notably, glutamine appears to be an important intermediary molecule between the neuronal and astrocytic compartment in the regulation of GABAergic inhibitory tone. Finally, we found that a deficiency in glutamine synthetase is an important pathogenic process for seizure generation in both the brain slice model and the human neuropathological study. Our study describes the first model for mitochondrial epilepsy and provides a mechanistic insight into how astrocytes drive seizure generation in mitochondrial epilepsy.

1 Institute of Neuroscience, Newcastle University, The Medical School, Framlington Place, Newcastle upon Tyne, NE2 4HH, UK
2 Wellcome Centre for Mitochondrial Research, Newcastle University, Institute of Neuroscience, The Medical School, Framlington Place, Newcastle upon Tyne, NE2 4HH, UK
3 Department of Drug Design and Pharmacology, University of Copenhagen, Copenhagen, 2100, Denmark
4 Department of Neurosurgery, Royal Victoria Infirmary, Newcastle upon Tyne, NE1 4LP, UK
5 Neural Pathways DPU, GSK, 11 Biopolis Way, 138667, Singapore
6 Discipline of Physiology, School of Medicine, Trinity College Dublin, Dublin 2, Ireland

†Present address: Neuroscience Drug Discovery Unit, Takeda Pharmaceuticals Limited, Shonan Research Center, 26–1, Muraoka-Higashi 2-chome, Fujisawa, Kanagawa 251–8555, Japan

Correspondence to: Mark O. Cunningham
Discipline of Physiology, School of Medicine, Trinity College Dublin, Dublin 2, Ireland
E-mail: mark.cunningham@tcd.ie

Keywords: mitochondrial epilepsy; astrocytes; glutamine synthetase; GABA-glutamate-glutamine cycle

Abbreviation: TLE = temporal lobe epilepsy

Received May 29, 2018. Revised September 30, 2018. Accepted October 29, 2018. Advance Access publication January 24, 2019

Introduction

With an estimated prevalence of about 1 in 4000, mitochondrial disease is one of the most common forms of adult inherited neurological disorders (Gorman *et al.*, 2015). Whilst mitochondrial disease involves a large number of neurological manifestations, approximately a quarter of the adult patient population have epilepsy (Whittaker *et al.*, 2015). Termed 'mitochondrial epilepsy', this specific subset of epilepsy is unique in that it is often super-refractory and typically has a poor prognosis in some patients (Bindoff and Engelsen, 2012). Though the epilepsy can manifest as virtually any seizure semiology and combination, the most commonly reported seizure type in the patient cohort as a whole was focal seizures (Bindoff and Engelsen, 2012; Chevallier *et al.*, 2014; Whittaker *et al.*, 2015). Additionally, mitochondrial epilepsy can manifest in conjunction with a wide range of phenotypes of mitochondrial disease. Epidemiological studies have reported though that epilepsy is most frequently associated with the m.8344A > G mutation that is associated with the syndrome myoclonic epilepsy with ragged red fibres (MERRF) and the most commonly reported genotype, m.3243A > G mutation that can cause the syndrome mitochondrial encephalopathy, lactic acidosis, and stroke-like episode (MELAS) (Whittaker *et al.*, 2015). Despite the well-characterized epileptic phenotype in clinical studies, there has been a lack of preclinical studies of mitochondrial epilepsy largely due to the paucity of a model of this epileptic syndrome.

A recent post-mortem neuropathological study on the neocortices of patients with mitochondrial epilepsy has shown profound interneuron loss and decreased expression of mitochondrial complex I and IV subunits in the remaining interneurons (Lax *et al.*, 2016). However, functional studies using *in vitro* brain slice electrophysiology have shown that the mere pharmacological inhibition of complex I or complex IV did not induce epileptiform discharges in the local field potential recordings, despite a severe reduction in the interneuron firing rate and the subsequent state of disinhibition (Kann *et al.*, 2011; Whittaker *et al.*, 2015). This discrepancy indicates that there is an additional pathogenic process beyond interneuron loss that contributes towards seizure generation in mitochondrial epilepsy. We hypothesized that this additional pathogenic process is mediated by astrocytes. To investigate this, we adopted a scientific framework (Chan *et al.*, 2016) where we examined the astrocytes in human neuropathological studies before extrapolating the finding to an *in vitro* brain slice setting and in turn, generating for the first time, a model of mitochondrial epilepsy. The model provided unique opportunity for dissecting the mechanisms involved in seizure generation in mitochondrial epilepsy, particularly concerning the astrocytic compartment.

Materials and methods

Patients and control cases for the neuropathology study

Eight patients with clinically or genetically defined mitochondrial disease, two patients with temporal lobe epilepsy (TLE) and eight control subjects were included in this neuropathological study (Table 1). Formalin-fixed paraffin-embedded (FFPE) occipital lobe blocks were obtained from the Newcastle Brain Tissue Resource (NBTR) and MRC Sudden Death Brain and Tissue Bank, Edinburgh. Ethical approval for the study was provided by Newcastle and North Tyneside Local Research Ethics Committee and all human tissue included in this study was used according to the Declaration of Helsinki.

Neurohistopathology and immunohistochemistry

The neuropathology of the patients included in this study has been previously described (Lax *et al.*, 2016). In the current study, 5 µm FFPE sections were taken from the occipital cortex and immunohistochemistry was performed to detect reactive astrocytes (anti-glial fibrillary protein, GFAP) (Dako Z0334) as previously described (Lax *et al.*, 2016).

Sequential COX/SDH histochemistry with immunofluorescent labelling of astrocytes

Frozen occipital sections (15 µm) were cut on a cryostat, mounted on to SuperFrost® slides and COX/SDH (cytochrome *c* oxidase/succinate dehydrogenase) histochemistry performed as previously described. Following immersion of slides into 100% ethanol, tissues were rehydrated and fixed for 15 min in cold 4% paraformaldehyde solution. Subsequently, sections were washed well with distilled water, and washed three times in Tris-buffered saline with Tween-20 (TBST). A blocking step consisting of 1% normal goat serum (NGS; Sigma) applied for 1 h at room temperature, followed by incubation with anti-GFAP at 1:1500 overnight at 4°C. The next day sections were washed three times in TBST and a secondary antibody applied (goat anti-rabbit IgG Alexa Fluor® 546 nm diluted 1:100) for 2 h at room temperature. The slides were washed three times with TBST and coverslips were mounted with ProLong® Gold (Life Technologies).

Quadruple immunofluorescent labelling of mitochondrial respiratory chain components in astrocytes

Immunofluorescence was performed on 5-µm thick FFPE sections of occipital tissue mounted on SuperFrost® slides. Immunofluorescence was performed on positive controls (all antibodies), no-primary-antibody (NPA) and no-secondary-antibody (NSA) controls for each of the four fluorophores to

Table 1 A detailed summary of all patients included in the neuropathological study

NBTR #	Patient	Age at death, years	Gender	Genetic defect	Symptoms	Migraine	Stroke-like episodes	Epilepsy	Age at onset (epilepsy)	Publications
2009/0061	m.3243A>G 1	20	F	m.3243A>G	MELAS		+	+		Lax *et al.*, 2012*b*, *c*, 2015; Reeve *et al.*, 2013; Chrysostomou *et al.*, 2015
2008/0038	m.3243A>G 2	30	M	m.3243A>G	Cardiomyopathy, PEO, diabetes	–	–	–	–	Chrysostomou *et al.*, 2015; Ng *et al.*, 2015
2010/0886	m.3243A>G 3	45	M	m.3243A>G	MELAS		+	+	41	Chrysostomou *et al.*, 2015; Lax *et al.*, 2015
2011/0065	m.8344A>G 1	58	M	m.8344A>G	MERRF	_	+	+	41	Reeve *et al.*, 2013; Chrysostomou *et al.*, 2015; Lax *et al.*, 2015
2004/0021	Single deletion 1	40	F	Single deletion	KSS	–	–	–	–	Lax *et al.*, 2012*a*, *b*, *c*, 2015; Reeve *et al.*, 2013
2001/0017	POLG 1	24	F	*POLG* (p.A467T and p.W748S)	CPEO, ataxia		+[a]	+	20	Lax *et al.*, 2011, 2012*b*, 2015; Reeve *et al.*, 2013
2010/0958	POLG 2	79	M	*POLG* (p.T251I; p.P587L and p.A467T)	CPEO, dysarthria, dysphagia		_	–		Chrysostomou *et al.*, 2015; Lax *et al.*, 2015
2011/0224	POLG 3	55	M	*POLG* (p.W748S and p.R1096C)	CPEO, ataxia, dementia, tremor	–	–	+	Childhood	Chrysostomou *et al.*, 2015; Lax *et al.*, 2015
681–12IL	TLE 1				TLE				11	
680–12A	TLE 2				TLE				Congenital	
SD0037–11	Control 1	48	M							
SD004–12	Control 2	61	M							
SD008–12	Control 3	25	M							
SD036–11	Control 4	48	M							
SD007–12	Control 5	48	M							
SD022–13	Control 6	45	M							
SD025–12	Control 7	47	M							
SD022–12	Control 8	44	M							

[a]Lax *et al.* (2012*c*).

CPEO = chronic progressive external ophthalmoplegia; F = female; M = male; MELAS = mitochondrial encephalopathy, lactic acidosis, and stroke-like episode; MERRF = myoclonic epilepsy with ragged red fibres; NBTR = Newcastle Brain Tissue Resource; PEO = progressive external ophthalmoplegia.

allow for background correction and cross-reactivity checks, respectively. Sections were deparaffinized and rehydrated by placement in a 60°C oven for 20 min, followed by immersion in Histo-Clear™ (National Diagnostics) and graded ethanol series (100% to 70%) to water. Antigen retrieval was performed using the 2100 retriever unit (Electron Microscopy Sciences©) which involved immersion of sections in 1 mmol EDTA (pH 8) and pressure cooking for 40 min. Sections were blocked in 1% NGS for 1 h at room temperature and incubated in primary antibodies at the optimal dilution overnight at 4°C. Mouse monoclonal primary antibodies used were directed against nuclear DNA-encoded respiratory chain complex subunits, NADH dehydrogenase [ubiquinone] 1 beta subcomplex subunit 8 (anti-NDUFB8; Abcam, ab110242) and cytochrome *c* oxidase subunit 1 (anti-COX1; Abcam, ab14703), and porin (anti-VDAC1; Abcam ab14734). A rabbit polyclonal antibody directed against GFAP was also applied. Following incubation with the primary antibodies, sections were washed with 10 mM TBS (3 × 5 min). Quadruple immunofluorescent labelling involved secondary anti-mouse antibodies conjugated with Alexa Fluor® 488 and 546, anti-rabbit conjugated with Alexa Fluor® 405 antibody or streptavidin-conjugated Alexa Fluor® 647 antibody (Life Technologies). The signal-to-noise ratio was increased by quenching the background signal with 3% Sudan Black for 10 min. Sections were then washed in distilled water and mounted with ProLong® Gold (Life Technologies).

Confocal microscopy and image processing

Astrocytes were imaged on *x*-, *y*- and *z*-planes using a point scanning confocal microscope (Nikon A1) using an immersion oil ×60 objective with numerical aperture of 1.4. Twenty-five GFAP-positive astrocytes were randomly sampled per case using an electronic zoom of ×3 (×180 magnification). *Z*-stacking was performed according to the recommended microscope settings (pixel size: 0.14 µm; *z*-step size: 0.17 µm; optical resolution: 0.13 µm and optical sectioning: 0.54 µm). Four lasers were used (405 nm, 488 nm, 561 nm and 647 nm), each detecting the signal from a different fluorophore. Microscope and laser settings were maintained throughout image capture.

To investigate complex I (NDUFB8), complex IV (COX1) and porin protein expression in GFAP-positive astrocytes, 3D images were analysed using Volocity® 3D image analysis (v.6.1.1, PerkinElmer). Regions of interest were manually drawn around each GFAP-positive astocyte and mitochondrial 'objects' were recognized within each region of interest, and protein intensity measurements were obtained from these.

Statistical analysis for the quadruple immunofluorescent labelling

Within astrocytes, the mean optical density values of NDUFB8, COX1 and porin immunofluorescence were measured (Volocity®, PerkinElmer) and background corrected. The background corrected optical density values were log transformed to normalize the data (yielding $NDUFB8_T$, $COX1_T$, and $porin_T$). The mean and standard error for distribution of $porin_T$ were estimated, as well as the regression parameters and the standard error of the estimate for the regression of $NDUFB8_T$ against $porin_T$ and $COX1_T$ against $porin_T$. For each area of interest, the z-score for the porin level was calculated, and the z-scores for NDUFB8 ($NDUFB8_Z$) and COX1 ($COX1_z$) were calculated using the linear regression based on the level of porin. Finally, astrocytes were classified based on standard deviation (SD) limits (for NDUFB8 and COX1: normal if $-2 < z < 2$ SD, low if $z < -2$ SD, deficient if $z < -3$ SD and very deficient if $z < -4$ SD). All statistical analyses were carried out using SAS 9.3 (Cary, NC).

Animal provision and use

For the majority of the work presented in this study, we used adult male Wistar rats aged 10–12 weeks, unless mentioned otherwise. The rats were procured from Charles River Laboratories and housed in the local animal housing unit at Newcastle University and University of Copenhagen (for the metabolic studies) under standard housing conditions. For a specific part of the presented study, we had used mice, specifically the adult male C57 Black 6 mice (C57BL/6) aged 8–10 weeks, obtained from the same supplier. All experimental and surgical procedures involving animals were carried out in accordance with the UK Animals (Scientific Procedures) Act 1986 with the internal approval of the Newcastle University Ethical Review Committee. For the metabolic study at the University of Copenhagen, all experimental procedures were in accordance with the Danish National Ethics Committee and the European Convention ETS 123 of 1986.

Patient cases for the electrophysiology study

Six patients with refractory epilepsy that underwent elective neurosurgical procedures were included in the electrophysiological study (Supplementary Table 1). All patients had given their written informed consent for use of the resected brain tissue prior to the surgical procedures. Ethical approval was provided by the County Durham and Tees Valley 1 Local Research Ethics Committee (06/Q1003/51; date of review 3 July 2006) and clinical governance was approved by the Newcastle upon Tyne Hospitals NHS Trust (CM/PB/3707). The use of all human tissue included in this study conformed to the Code of Ethics of the World Medical Association (Declaration of Helsinki) as printed in the British Medical Journal (18 July 1964).

In vitro brain slice preparation

Rodents were given the inhaled anaesthetic isoflurane (IsoFlo®, Abbott Laboratories Ltd) and following loss of consciousness, they were administered intramuscular injection of a mixture of ketamine (0.3 ml for rat and 0.15 ml for mice) (Narketan® 100 mg/ml, Vetoquinol) and xylazine (0.3 ml for rat and 0.15 ml for mice) (Xylacare® 20 mg/ml, Animalcare). Once reflexes had disappeared, rodents were transcardially perfused with ice-cold oxygenated (95% O_2/ 5% CO_2) sucrose artificial CSF (containing 3 mM KCl, 1.25 mM NaH_2PO_4, 2 mM $MgSO_4$, 2 mM $CaCl_2$, 24 mM $NaHCO_3$, 10 mM glucose and 252 mM sucrose). They were then decapitated and the brains

were removed quickly. The cerebellum was removed and the remaining brain was sliced along the horizontal axis to 450-µm thick slices using the 5100 mz Vibratome (Campden Instruments). Slices were then collected and trimmed down leaving behind the hippocampus and the parahippocampal cortices. Slices were then transferred into a holding chamber and maintained at an interface between normal artificial CSF (containing 126 mM NaCl, 3 mM KCl, 1.25 mM NaH_2PO_4, 1 mM $MgSO_4$, 1.2 mM $CaCl_2$, 24 mM $NaHCO_3$, and 10 mM glucose) and carbogen gas at room temperature for 1 h to equilibrate.

Human tissue collection and slice preparation

Human tissue was collected as described previously (Roopun *et al.*, 2010; Cunningham *et al.*, 2012; Simon *et al.*, 2014). Following removal of the resected tissue, it was immediately transferred to a beaker containing oxygenated ice-cold sucrose artificial CSF and transported to the laboratory within 5 min. The tissue was sliced into 450-µm thick slices using the Microm HM 650 V vibratome (Thermo Fisher Scientific) and incubated in the holding chamber as described above.

Electrophysiological experiment set-up

Slices were transferred into an interface recording chamber and maintained at a 30–33°C temperature range at an interface between the normal artificial CSF and humidified carbogen gas. The circulation of normal artificial CSF was maintained using a SciQ 400 series pump (Watson Marlow) at a rate of 1–1.2 ml/min. Slices were allowed to adjust to the chamber condition for 30 min before any experiments were initiated. Extracellular electrodes were prepared by pulling micropipettes from a thin-walled borosilicate glass pipette (1.2 mm outer diameter × 0.94 mm inner diameter, Harvard Apparatus Ltd) using a PP-83 puller (Narishige). These electrodes were then filled with normal artificial CSF and placed in the stratum pyramidale layer of the CA3 subregion of the hippocampus. Local field potentials were recorded using the extracellular electrodes, which were connected to a pre-amplifier EXT-10/2F headstage (Npi Electronics). The signal was then band pass filtered between 10 Hz and 100 Hz by the AI-2130 differential amplifier (Axon Instrument, Molecular Devices) and the mains electrical noise was eliminated using the Hum-Bug noise eliminator (Quest Scientific Instruments). The analogue signal obtained was digitized at 5 kHz using the ITC-16 multi-channel data acquisition interface (Digitimer). The local field potential was then recorded using the AxoGraph X software (Axograph Scientific) on a Macbook Pro computer (Apple). Data were analysed off-line with Microsoft Excel (Microsoft Inc., USA), MATLAB 2010a (MathWorks, USA), and Prism 7.0 (GraphPad Software, USA). An automated script was written in MATLAB to enable automated detection of epileptiform discharges using a threshold value. A 10-min portion of the recording was analysed in any one time and the value of burst count was expressed as the amount of epileptiform discharges per minute.

Drugs

The drugs used in this study are listed in Supplementary Table 2. Drugs were dissolved according to the supplier's instructions. Whenever possible, stock solutions of the drugs were prepared by dissolving in distilled H_2O. Otherwise, drugs were dissolved in dimethyl sulphoxide (Sigma Aldrich) with a final concentration of $<1\%$ v/v. Stock solutions of the drugs were either kept at 4°C or frozen at −20°C in aliquots according to the supplier's instructions.

Post hoc immunohistochemistry

Following the electrophysiological recordings, slices were fixed in 4% paraformaldehyde in 0.1 M phosphate-buffered saline and stored at 4°C. Control slices were incubated in the holding chamber for the same duration of time as the fixed experimental slices. One day before processing, slices were removed from the paraformaldehyde and placed in TBS solution containing 30% sucrose for overnight cryoprotection. Slices were then resectioned to 40-µm thick sections using a freezing stage microtome (Shandon Life Sciences International). Antigen retrieval was then conducted by two 5-min incubations in microwave-boiled 50 mM sodium citrate solution at pH 6.0. Following three TBS washes, the endogenous peroxidase was quenched by incubation in 0.3% hydrogen peroxide in 70% methanol in TBS solution at room temperature for 1 h. After another three TBS washes, sections were incubated in a 1% casein in TBS solution for 1 h. This was followed by three TBS washes and then incubated in 0.05% Tween in TBS (TBST) solution for 10 min. The sections were then incubated in the primary antibody diluted in 0.05% TBST solution and 5% corresponding normal serum (for a list of antibodies refer to Supplementary Table 3). Following the overnight incubation, sections were incubated for 2 h at room temperature on a rocking platform. Sections then underwent three TBS washes and incubated in the appropriate secondary antibodies diluted to 1:200 in 0.05% TBST solution for 2 h at room temperature. This was again followed by three TBS washes and subsequently by incubation in horseradish peroxidase (Ready-To-Use Streptavidin Horseradish Peroxidase, VectorLabs) for 2 h at room temperature. Following another three TBS washes, the section was incubated in DAB (SigmaFast® DAB tablets, Sigma Aldrich) in TBS solution for 5 min. This was then followed by a final three TBS washes and sections were then mounted onto gelatine-subbed glass slides. After air-drying overnight, slides were washed in distilled water before being dehydrated by incubation in sequential ethanol concentration gradients; starting from 70%, 95%, and 100%. Sections were then bathed in Histoclear (National Diagnostics) for 10 min before being cover-slipped using the DPX Mounting Media (Fisher Scientific). Unless otherwise mentioned, all the reagents were obtained from Sigma Aldrich.

Microscopy and quantification

Microscope slides were examined under a stereology light microscope Olympus BX51 (Olympus Corporation). Quantification was performed using the software Stereo Investigator (MBF Bioscience). An outline was drawn at 2.5× magnification around the hippocampus CA3. The area of this outline was calculated and a meander scan was then

performed at 20× magnification to allow for sequential scanning and cell counting for each portion of the region until the whole region was counted. The entire cell population for the region was sampled according to the criteria of a clear and visible nuclear and cytoplasmic profile. The obtained cell count was divided by the area to generate the cell density (cells/mm^2).

Metabolic incubation

The metabolic incubation set-up and the subsequent analysis was performed according to previously published protocol with slight modification (McNair *et al.*, 2017). For the metabolic incubation experiments, slices were 300-µm thick instead and trimmed down to contain only the hippocampus. These hippocampal slices were then immediately transferred to the recording chamber where four hippocampal slices were placed on each chamber. The recording chamber was maintained as above at a temperature range of 30–33°C at an interface between the carbogen gas and the normal artificial CSF. Normal artificial CSF (20 ml) was circulated constantly using a SciQ 400 series pump (Watson Marlow) at a rate of 1–1.2 ml/min. Slices were allowed to equilibrate to the chamber condition for 30 min. They were then exposed to 0.1 mM fluorocitrate for 30 min, after which they were exposed to 500 nM rotenone and 10 µM potassium cyanide for 30 min. This pre-incubation condition was designed to resemble the protocol for the mitochondrial respiratory challenge and the slices have been proven to be 'epileptic' at this stage of the incubation. Control slices were pre-incubated with the respective vehicles. Slices were gently rinsed with warm glucose-free normal artificial CSF before they were transferred to the experimental medium to incubate for 1 h. The experimental medium consisted of normal artificial CSF where 10 mM glucose was substituted for 10 mM [U-13C]-glucose (Cambridge Isotope Laboratories, CLM-1396) with supplemental composition depending on the treatment group. The control group was supplemented with the vehicles; the epileptic group was supplemented with the epileptogenic cocktail mixture; epileptic + 2.5 mM glutamine was supplemented with the epileptogenic cocktail mixture and 2.5 mM glutamine; and epileptic + 2.5 mM GABA was supplemented with the epileptogenic cocktail mixture and 2.5 mM GABA. In all conditions, the final volume of the medium was kept to 20 ml. Incubations were terminated after 1 h and the slices were gently rinsed with ice-cold glucose-free normal artificial CSF and then put into 5 ml of ice-cold 70% ethanol. The slices were then homogenized using ultrasonication (Fisher Scientific, FB120) at 25% amplitude with temperature setting at 15°C and total sonication time of 45 s with a 2 s on and 3 s off cyclic interval. Samples were kept on ice at all times during the sonication to prevent heating and denaturation of the samples. Samples were then centrifuged at 20 000*g* for 20 min at 4°C. The supernatant was then taken as the 'extract' sample and stored at −80°C. The pellets were dried at room temperature overnight to allow excess ethanol to evaporate. These pellets were then reconstituted in 500 µl 1 M KOH for at least 8 h at room temperature and the protein concentration was determined using the Pierce BCA Protein assay-kit (Thermo Fisher Scientific) as per the supplier's instruction.

High performance liquid chromatography and gas chromatography mass spectrometry

This analytical technique was conducted according to a previously published protocol (McNair *et al.*, 2017). The high performance liquid chromatography (HPLC) technique was used to determine the tissue amount of the amino acids. Gas chromatography mass spectrometry (GC-MS) was used to determine the incorporation of the ^{13}C labelling into various metabolites following the metabolism of the substrate [U-13C]-glucose.

Immunofluorescent analysis of glutamine synthetase content in astrocytes

FFPE sections (5 µm) were dual-labelled immunofluorescently for GFAP and glutamine synthetase (GS; BD 610517) as previously described. The only exceptions were: antigen retrieval was performed by immersing sections in 0.1 M citrate buffer (pH 6) and microwaving for 10 min, followed by 10 min of cooling. Primary antibodies, anti-GFAP and anti-GS, were applied at 1:1000 and 1:8000 followed by an anti-rabbit-IgG Alexa Fluor® 546 nm and anti-mouse IgG2a Alexa Fluor® 488 nm to label astrocytes and glutamine synthetase, respectively.

Confocal microscopy, image processing and analysis for glutamine synthetase

Astrocytes were imaged on *x*-, *y*- and *z*-planes using an inverted point scanning confocal microscope (Nikon A1R). Areas of interest were detected using an immersion oil ×60 objective with numerical aperture of 1.4. Twenty astrocytes were randomly sampled per case using an electronic zoom of ×3 (×180 magnification). *Z*-stacking was performed according to the recommended microscope settings (pixel size: 0.14 µm; *z*-step size: 0.17 µm; optical resolution: 0.13 µm and optical sectioning: 0.54 µm). Three lasers were used (405 nm, 488 nm, and 561 nm), each detecting the signal from a different fluorophore. Microscope and laser settings were maintained throughout image capture.

To investigate glutamine synthetase protein expression in astrocytes, 3D images were analysed using Volocity® 3D image analysis software (v.6.1.1, PerkinElmer). This involved detection of GFAP-positive astrocytes based on the 546 nm signal and measuring the mean optical densities for glutamine synthetase (488 nm signal).

Statistical analysis

All statistical analyses were performed using GraphPad Prism 7.0 (GraphPad Software, Inc). For the immunohistochemical and the biochemical data, a two-tailed unpaired *t*-test was performed when two groups were compared and a one-way ANOVA was performed when multiple groups were compared. For the electrophysiological data, a two-tailed paired

t-test was carried out when two groups were compared and a one-way ANOVA with repeated measures was performed when multiple groups were compared. For the neuropathological study, a one-way ANOVA was performed to compare individual patient's glutamine synthetase optical density with control values. All the data were subjected to the Shapiro-Wilk normality test to determine if the data came from a Gaussian distribution. When the data were not normally distributed, an equivalent non-parametric test was performed in place of the tests mentioned earlier. A significant *P*-value cut-off was taken at $*P \leqslant 0.05$, $**P \leqslant 0.01$, and $***P \leqslant 0.001$. Sample size was determined based on previous experience with the data. For detailed statistical information on the data presented in this study, see Supplementary Table 4.

Data availability

All the data included in this study are available and will be provided transparently upon request to the corresponding author.

Results

Astrogliosis is associated with grey matter lesions in patient tissues

Eight adult patients with mitochondrial disease were included in the current study, comprising three patients with m.3243A>G mutation, one patient with m.8344A>G mutation, one patient with a single large scale mitochondrial DNA deletion, and three patients with autosomal recessive POLG mutations. The clinical summaries are given in Table 1. Three of these patients did not have a history of epilepsy, namely Patients m.3243A>G 2, single deletion 1, and POLG 2. The remaining five had recorded clinical history of epilepsy. Eight age-matched male control patients with no known history of neurological disorders were included in this study as direct comparison. As the occipital cortex has previously shown neuropathological changes (Lax *et al.*, 2016), we sought to further characterize astrogliotic changes in this cortical region. Areas of focal neuronal necrosis were evident in the occipital cortex of three out of the eight patients with mitochondrial disease (Patients m.3243A>G 2, m.3243A>G 3 and m.8344A>G 1). In the other patients with mitochondrial disease, there was more diffuse neuronal cell loss and atrophy of the cortical ribbon. Hippocampal sclerosis was evident in patients with TLE. In those areas associated with neurodegeneration, proliferation of reactive astrocytes was observed by GFAP-positive staining (Fig. 1A).

Astrocytes are respiratory deficient for complexes I and IV

Since COX/SDH histochemistry revealed the presence of COX-deficient SDH-positive cells, which were identified as GFAP-positive in tissues obtained from patients (Supplementary Fig. 1), a quadruple immunofluorescent assay was developed to quantify the degree of respiratory chain deficiency occurring in GFAP-reactive astrocytes. Assessment of mitochondrial mass marker porin revealed lower mitochondrial densities in astrocytes relative to neurons. Immunofluorescent labelling of mitochondrial respiratory chain protein subunits NDUFB8 and COX1 for complexes I and IV, respectively, relative to mitochondrial mass marker porin within GFAP-positive astrocytes revealed colocalisation in control subjects (Fig. 1B). In patients with mitochondrial disease, there appears to be decreased expression of NDUFB8 and COX1 relative to porin in GFAP-positive astrocytes, a finding that is indicative of respiratory chain deficiency. Quantification of optical densities for each marker provided evidence that the mitochondria within astrocytes show downregulation of subunits of complexes I and IV in patients with mitochondrial disease and patients with TLE. Complex I (NDUFB8 subunit) expression was predominantly affected with reduced levels detected in all patients, and z-scores suggestive of deficiency affecting six of the eight patients with mitochondrial disease (Fig. 1C). Complex IV (COX1 subunit) expression was more preserved in patients with mitochondrial disease, with only three of the eight demonstrating z-scores corresponding to deficiency (Fig. 1D). The reduction in complex I and IV subunit expression in astrocytes was evident in patients with mitochondrial disease whether they had epilepsy or not. In patients with TLE, the pattern of deficiency is similar to the patients with mitochondrial disease with predominant complex I expression deficiency and a subtler deficiency of complex IV expression.

Development of the novel *in vitro* brain slice model of mitochondrial epilepsy

Based on the neuropathological findings, we hypothesized that functional inhibition of astrocytes may be an important pathogenic process in the generation of mitochondrial epilepsy. To recapitulate this *in vitro*, we used a pharmacological agent that could selectively inhibit astrocytic function. Fluorocitrate is a well-characterized selective inhibitor of astrocytic aconitase, an enzyme of the TCA cycle responsible for the conversion of citrate to isocitrate (Hassel *et al.*, 1992; Swanson and Graham, 1994). We then combined the acute application of fluorocitrate, with inhibitors of the mitochondrial respiratory chain complex I and IV, rotenone and potassium cyanide, respectively, onto acute hippocampal slices to examine if such a combination would produce epileptiform discharges. Since the inhibitory effect of fluorocitrate hinges on the uptake of the citric compound into the astrocytes (Fonnum *et al.*, 1997), we chose to pre-incubate slices in 0.1 mM fluorocitrate for 60 min prior to the mitochondrial respiratory challenge. Following pre-

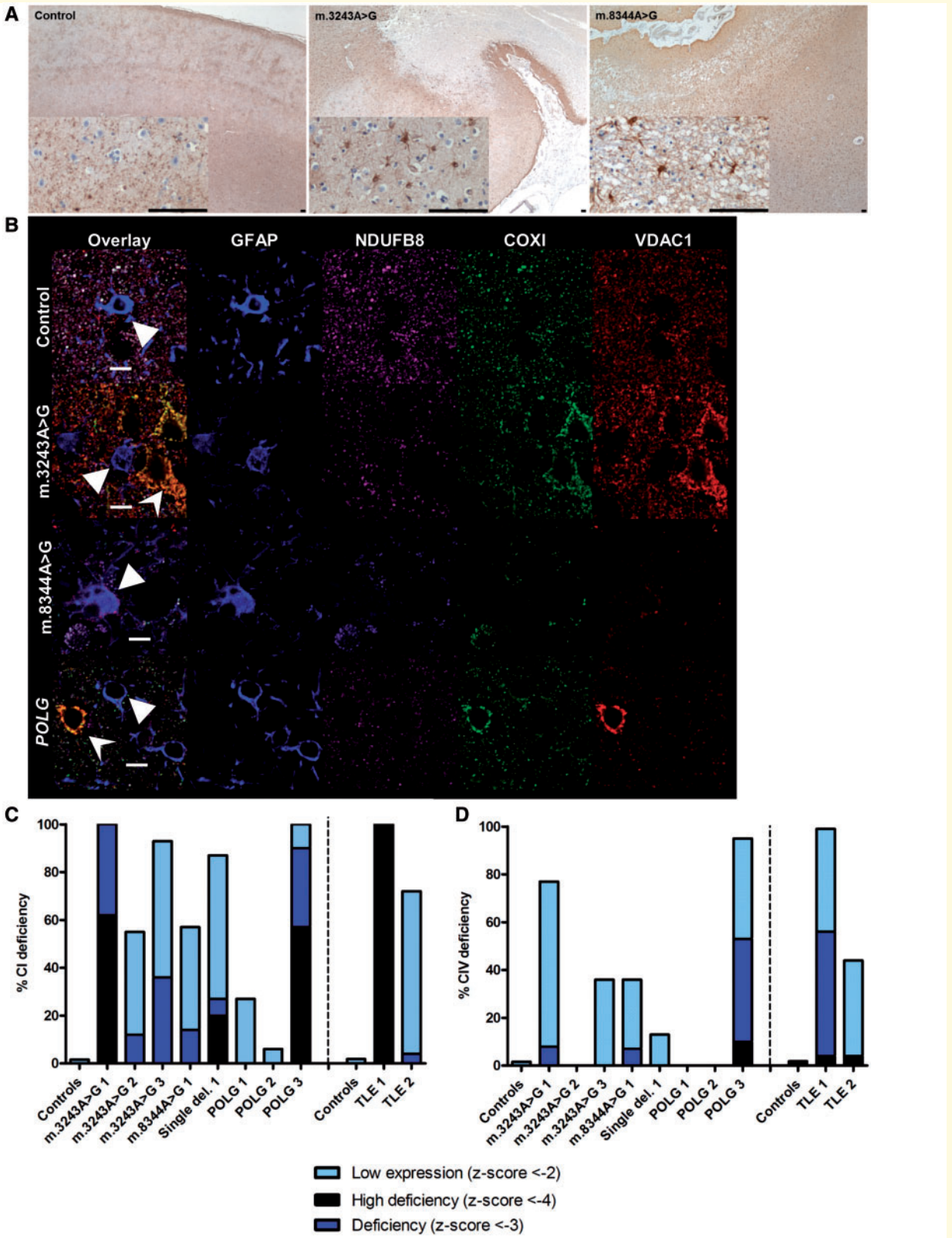

Figure 1 Proliferation of reactive astrocytes occurs in areas affected by neuronal cell loss and astrocytes show evidence of mitochondrial respiratory chain defects. Astrocytes are present in control cortex, mainly associated with blood vessels, while patients with m.3243A > G and m.8344A > G show evidence of astrogliosis in areas of the cortex that have undergone neurodegeneration (**A**). Scale bar = 100 μm. Astrocytes from control subjects show matched co-localization of NDUFB8, COX1 and porin, while patients with mitochondrial disease and TLE astrocytes show evidence of reduced NDUFB8 and COX1 immunolabelling (**B**). Scale bar = 10 μm. Graphs show quantification of mean optical densities for NDUFB8 (**C**) and COX1 (**D**) expression within astrocytes. Each bar is colour-coded according to level of expression (black = very deficient; dark blue = deficient; light blue = low).

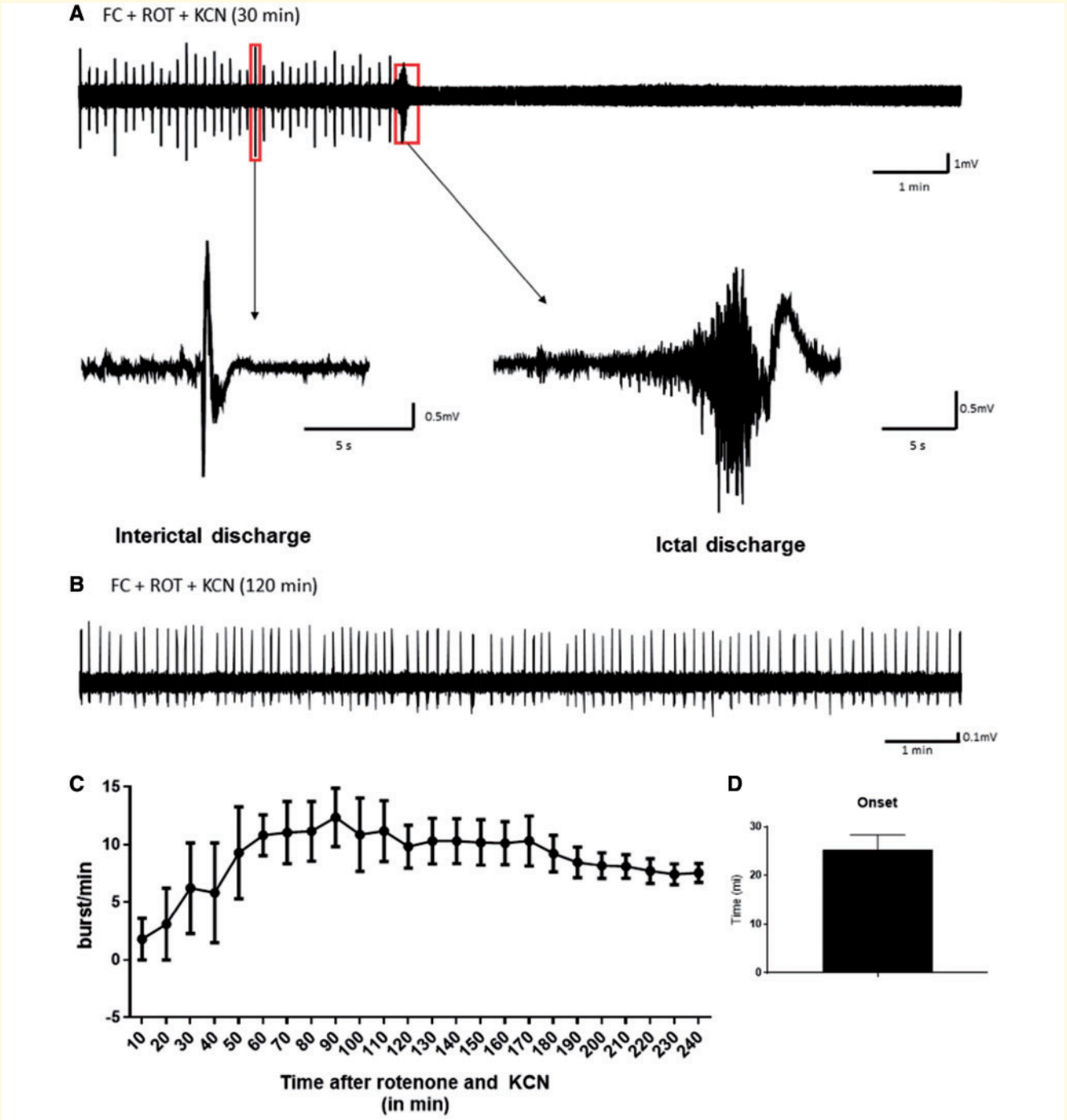

Figure 2 Epileptic activity was inducible *in vitro* in rodent hippocampus CA3 using a combination of the astrocytic aconitase inhibitor, fluorocitrate, and the mitochondrial respiratory complex I and IV inhibitors, rotenone and potassium cyanide. Robust epileptiform discharges are induced through a 60 min preincubation with 0.1 mM fluorocitrate (FC) followed by a challenge with respiratory complex I inhibitor, rotenone (ROT, 500 nM); and complex IV inhibitor, potassium cyanide (KCN, 10 μM). For the first 2 h of the challenge with the inhibitors, a typical cyclic pattern of the epileptiform discharge is observed as indicated in the representative trace (**A**). The cycle initiates with interictal discharges that build up and amount to a high frequency ictal discharge. This prominent ictal discharge is followed by a period of post-ictal silencing after which interictal discharges initiate again. Over time, this cyclic pattern transitions into a phase where only recurrent interictal discharges are observed with the absence of the ictal discharge, as exemplified by the representative trace (**B**). This stage of the activity typically occurs after 120 min of the epileptiform discharge development, after which a period of stable recurrent interictal discharge is achieved. The graph (**C**) depicts the evolution of this activity over time by means of a quantifiable parameter of the epileptic activity, burst count (or frequency) (n = 5). The onset of the seizure (n = 5) was quantified and presented in the bar chart (**D**).

incubation, slices were exposed to the concomitant application of 500 nM rotenone and 10 μM potassium cyanide. This combination of pharmacological agents was able to induce epileptiform discharges in CA3 of rodent hippocampal slices (Fig. 2A and B) with a mean onset of epileptiform discharges at 25.31 ± 3.06 min following the mitochondrial respiratory challenge (Fig. 2D). Within the first 120 min following the mitochondrial respiratory challenge, the epileptiform discharges manifested in a cyclic pattern of intermittent interictal discharges followed by a large burst of high frequency ictal discharges with a subsequent period of post-ictal silencing before re-manifesting as interictal discharges (Fig. 2A). After 120 min, the network discharges shifted towards a stable state of late recurrent interictal discharges characterized by the absence of the ictal discharges (Fig. 2B). This evolution of the epileptiform discharges could also be observed from the measures of the burst count showing achievement of steady state following 120 min of mitochondrial respiratory challenge and sustainability of up to 5 h after the initial challenge (Fig. 2C). These epileptiform discharges were not observed with the application of the mitochondrial respiratory challenge alone or the application of the astrocytic inhibitor fluorocitrate alone. The mitochondrial respiratory challenge was also interchangeable with equivalent respiratory chain inhibitors. Equimolar substitution of rotenone with MPP^+ iodide or potassium cyanide with sodium azide still generated a similar pattern of epileptiform discharges following the pre-incubation with fluorocitrate (Supplementary Fig. 2). Higher concentrations of the mitochondrial respiratory inhibitors (1 μM rotenone and 100 μM potassium cyanide) led to the generation of a generalized cortical spreading depression instead of epileptiform discharges (Supplementary Fig. 3). Additionally, we have also demonstrated that the protocol induces similar pattern and evolution of epileptiform discharges in acutely prepared mice brain slices (Supplementary Fig. 4), suggesting cross-species applicability of the model. Therefore, the aforementioned conditions represented the most optimal conditions for the generation of mitochondrial epileptiform discharges *in vitro*.

Applicability to human brain slices

This protocol for *in vitro* mitochondrial epileptiform induction also produced a similar pattern of epileptiform discharges in acutely resected human brain slices from six patients undergoing elective neurosurgical procedures for either refractory TLE or brain tumours (Supplementary Fig. 4 and Supplementary Table 1). Prior to the induction of mitochondrial epilepsy, local field potential recordings from these human brain slices demonstrated the absence of any spontaneous epileptiform activity. This finding is vital as this proves the translatability of the rodent brain slice model to a human brain slice setting and suggests a common pathogenic mechanism in the generation of mitochondrial epilepsy between rodents and humans.

The model recapitulates the observation from the human neuropathological study

Since the *in vitro* brain slice model is largely based on the observations from the human neuropathological study, it is imperative that the brain slice model recapitulates the neuropathological features observed in patient tissue. We therefore examined changes in different cellular populations of the hippocampal brain slices following 2 h of mitochondrial respiratory challenge using *post hoc* immunohistochemistry. There was a significant loss of neurons in the hippocampus CA3 region in the epileptic slices as compared with controls (Fig. 3A and D) as evidenced by the significant loss of NeuN expression in the epileptic slices. The reduced expression of the neuronal marker NeuN represented acute neuronal death rather than the loss of antigenicity due to the nature of the expression of the NeuN protein (Gusel'nikova and Korzhevskiy, 2015). We further demonstrated that excitatory pyramidal cell populations were relatively spared by the epileptic induction (Fig. 3B and E) while the inhibitory GABAergic cell populations were significantly reduced in the epileptic slices (Fig. 3C and F). We further confirmed the loss of inhibitory interneurons by examining the expression of three interneuron markers: parvalbumin, calbindin, and calretinin; and found significant reduction of expression of these markers in the epileptic slices (Supplementary Fig. 5). Together, these findings suggest the selective vulnerability of the inhibitory interneuron population in response to the mitochondrial epilepsy challenge, which closely resembles previous observation in a human neuropathology study (Lax *et al.*, 2016). The astrocytic population, as indicated by GFAP expression, was also affected by the mitochondrial epilepsy induction. In the control tissues, astrocytes were observed to be present in an organized and laminar manner across all layers of the tissue (Fig. 3G). In contrast, in the epileptic tissues, prominent glial scars were found in both the neocortex and the hippocampus. These glial scars were well defined and encapsulated with no viable astrocytes observed at the core of the lesion (Fig. 3H and J). Quantification of GFAP expression confirmed a significant upregulation of astrogliosis in the epileptic state (Fig. 3I). The presence of glial scars is indicative of end-stage severe reactive astrogliosis (Sofroniew, 2009) and recapitulates the aforementioned reactive pattern of astrogliosis seen in the human neuropathology studies (Fig. 1A).

Induced mitochondrial epilepsy in this model demonstrates extreme pharmacoresistance against conventional antiepileptic agents

Various clinical studies have reported that patients with mitochondrial epilepsy tend to respond poorly to

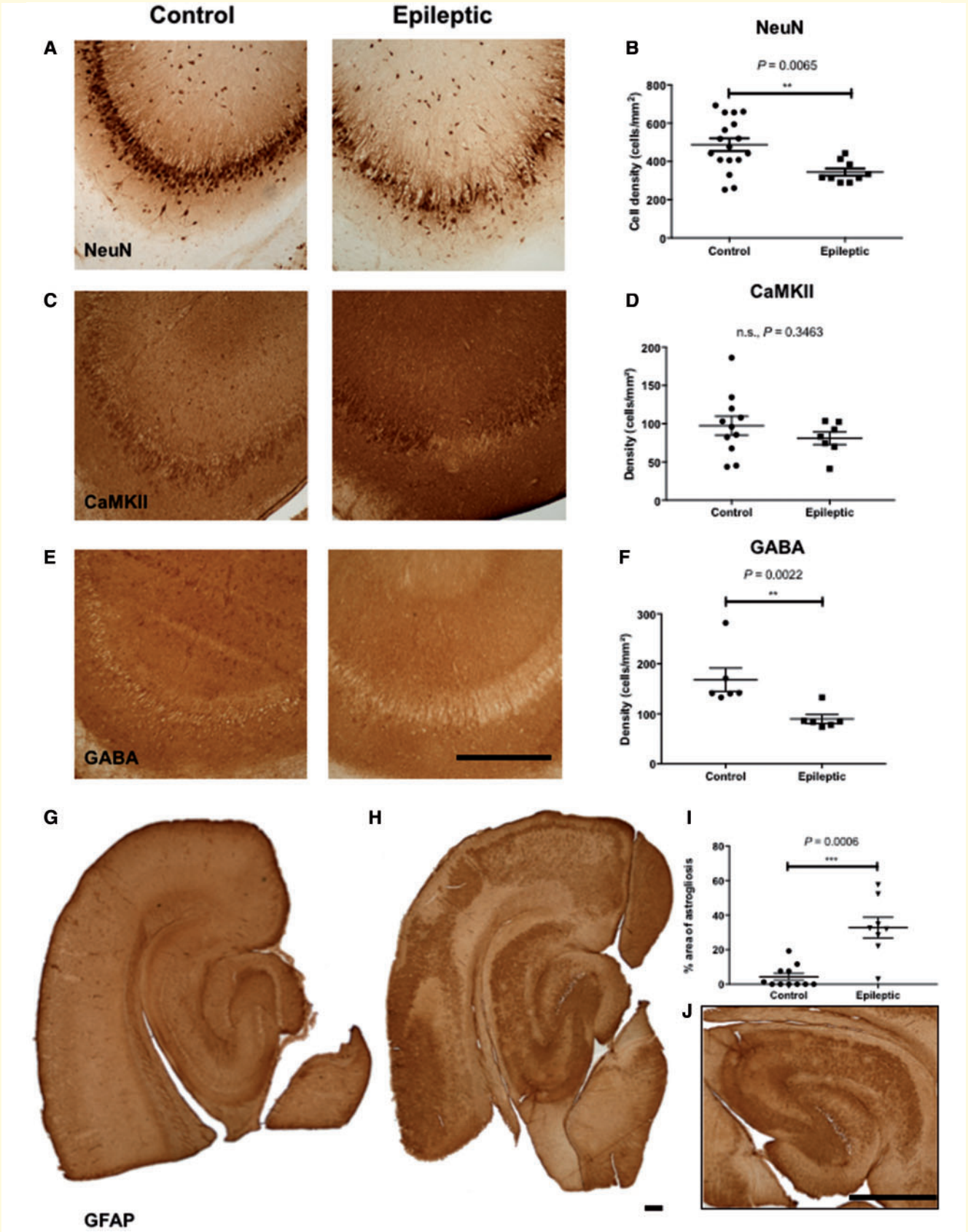

Figure 3 Similar neuropathological changes were observed in the *in vitro* brain slice model as was seen in the human study, including interneuron loss and reactive astrogliosis. A significant loss of neurons (**A**) is observed in the epileptic hippocampus slice as compared to control. There appears to be a relative sparing of the excitatory pyramidal cell population (**C**) and neuronal loss seems to be

(continued)

conventional antiepileptic agents and even if early seizure control is achievable, epileptic phenotypes resurface and are frequently progressive (Khurana *et al.*, 2008; Bindoff and Engelsen, 2012; Finsterer and Mahjoub, 2013; Whittaker *et al.*, 2015). Since pharmacoresistance is characteristic of mitochondrial epilepsy, we examined the response of the epileptiform activity in our model against conventional antiepileptic agents from various subgroups; including the sodium channel blockers: carbamazepine, lamotrigine, and phenytoin; benzodiazepines: midazolam and lorazepam; levetiracetam, barbiturates (sodium pentobarbital), and valproate. Two concentrations were chosen to represent the minimal inhibitory concentration (MIC) and the maximal tolerable concentration (MTC) based on previously reported predicted clinical exposures. There was no significant inhibitory response recorded by the application of the MIC of these antiepileptic agents (Fig. 4A) but upon application of the MTC, there was a significant inhibition of the epileptiform discharges afforded by the barbiturate, sodium pentobarbital (Fig. 4B). Although the barbiturate at MTC was capable of suppressing the epileptiform discharges, it was striking that none of the other antiepileptic agents had any significant suppressive effect at their MTC. These pharmacological results support the refractory nature of the induced mitochondrial epileptiform discharges in this model.

GABA deficiency underlies the failure of benzodiazepine to suppress pathological activity

Both benzodiazepines and barbiturates are well characterized allosteric modulators of the $GABA_A$ receptor, albeit with different binding sites (Greenfield, 2013). Barbiturates, however, can directly activate the $GABA_A$ receptor, even in the absence of GABA, whereas benzodiazepines cannot (Rho *et al.*, 1996). Considering the previously demonstrated observation that there are reductions in the inhibitory tone in neuronal microcircuits in epileptic slices (Fig. 3C and F), we examined if this deficiency of GABA in epileptic slices contributes to the resistance observed towards benzodiazepines. Firstly, we found that the application of GABA alone was able to afford a significant suppressive effect at the concentration of 2.5 mM, but not at 0.5 mM (Fig. 4C). To test the aforementioned hypothesis, we applied the lower concentration of GABA (0.5 mM) concomitantly with the MIC of the benzodiazepine, lorazepam (50 μM). Compared with the lack of inhibitory response observed by the application of either of these compounds alone, the concomitant application of GABA and lorazepam produced a synergistic inhibitory effect affording significant seizure suppression (Fig. 4D). This suggests that the lack of response of the induced epileptiform discharges in this model towards a benzodiazepine is primarily attributable to the deficiency of GABA in the epileptic tissue.

GABA deficiency in the epileptic tissue is a consequence of the downregulation of the astrocytic GABA-glutamate-glutamine cycle

The GABA-glutamate-glutamine cycle is a vital process implicated in the recycling of both the excitatory neurotransmitter, glutamate, and the inhibitory neurotransmitter, GABA, via the non-neuroactive precursor molecule, glutamine (Bak *et al.*, 2006). This cycle involves both the neuronal and astrocytic compartments but the synthesis and release of glutamine as precursor for the neurotransmitters are confined to the astrocytes. To understand the contribution of the GABA-glutamate-glutamine cycle to the pathology of this model, we examined the response of the epileptiform discharges towards the application of glutamine and glutamate. There was no significant change in the epileptiform discharges upon the application of glutamate (Fig. 4E) but a significant seizure suppression was achievable by the application of the high concentration of glutamine (2.5 mM) (Fig. 4F). To confirm the role of the astrocytic part of the GABA-glutamate-glutamine cycle, we measured the amount of glutamate and glutamine in the epileptic tissue as compared against non-epileptic control tissue using HPLC. The HPLC measurements showed a significant reduction of glutamine in the epileptic tissue (Fig. 5A) but no difference in the levels of glutamate between control and epileptic tissue (Fig. 5B). These data correspond with the functional responses of the application of the substrates in the mitochondrial epilepsy model, whereby the suppression of seizures was observed only with glutamine application. To provide further evidence

Figure 3 Continued
selectively confined to GABAergic inhibitory cells (**E**). Scale bar = 100 μm (**A**, **C** and **E**). Graphs (**B**, **D** and **F**) show quantification of cell density of the expression of the neuronal markers NeuN (n = 17 control, n = 9 epileptic), CaMKII (n = 11 control, n = 7 epileptic), and GABA (n = 6 control, n = 6 epileptic) in the control and epileptic slices. Reactive astrogliosis is also evidenced in the epileptic slices (**H**), whilst largely absent in the control slices (**G**). Quantification of the percentage area of astrogliosis (n = 11 control, n = 8 epileptic) within each slice, depicted in the graph (**I**), showed significant upregulation of gliosis in the epileptic slices. The inset (**J**) shows a typical astrogliotic pattern in the epileptic slices with a scar-forming gliosis along a focal well circumscribed area of lesion within the hippocampus CA3. This same pattern is also observable in the neocortex of such epileptic slices. Scale bar (inset) = 100 μm. $^{**}P \leqslant 0.01$, $^{***}P \leqslant 0.001$.

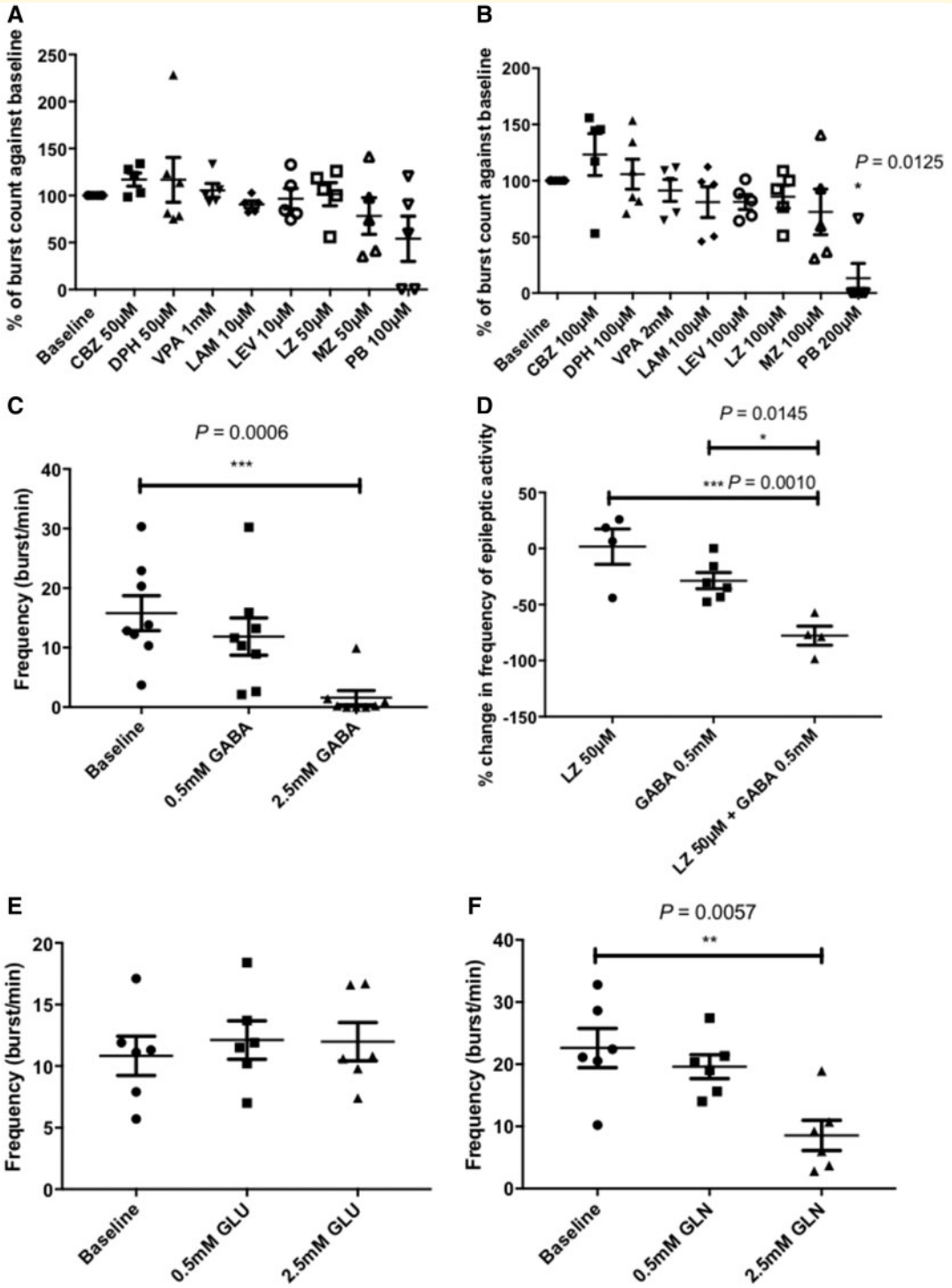

Figure 4 Pharmacoresistance is observed with the epileptiform discharges in the *in vitro* model and implicates involvement of the astrocytic GABA-glutamate-glutamine cycle in the regulation of GABA-ergic inhibition in this model. The addition of a variety of conventional antiepileptic drugs at their reported minimal inhibitory concentration (**A**) has elicited minimal inhibitory response in the interictal discharges. At the suprathreshold concentration (**B**), minimal response is still observed with the majority of the tested antiepileptics except for pentobarbital, which was able to afford significant suppressive effect ($n = 6$ for baseline and phenytoin, $n = 5$ for all other treatment groups). The addition of GABA (**C**) was also able to afford significant suppression at the high concentration of 2.5 mM ($n = 8$). When co-applied with the benzodiazepine lorazepam, the lower concentration of GABA (0.5 mM) was able to produce a synergistic effect creating a maximal inhibitory effect towards the interictal discharges (**D**) ($n = 4$ for lorazepam and lorazepam + GABA group, $n = 6$ for GABA group). As GABA is synthesized via the intermediary of the astrocytic GABA-glutamate-glutamine cycle, substrates of this cycle were tested for its anticonvulsant properties in this model. Interestingly, addition of glutamate (**E**) was unable to afford any suppressive effect whereas glutamine (**F**) was able to exert a significant anticonvulsant property at the equimolar concentration as GABA ($n = 6$ for glutamate, $n = 5$ for glutamine). $^{*}P \leqslant 0.05$, $^{**}P \leqslant 0.01$, $^{***}P \leqslant 0.001$.

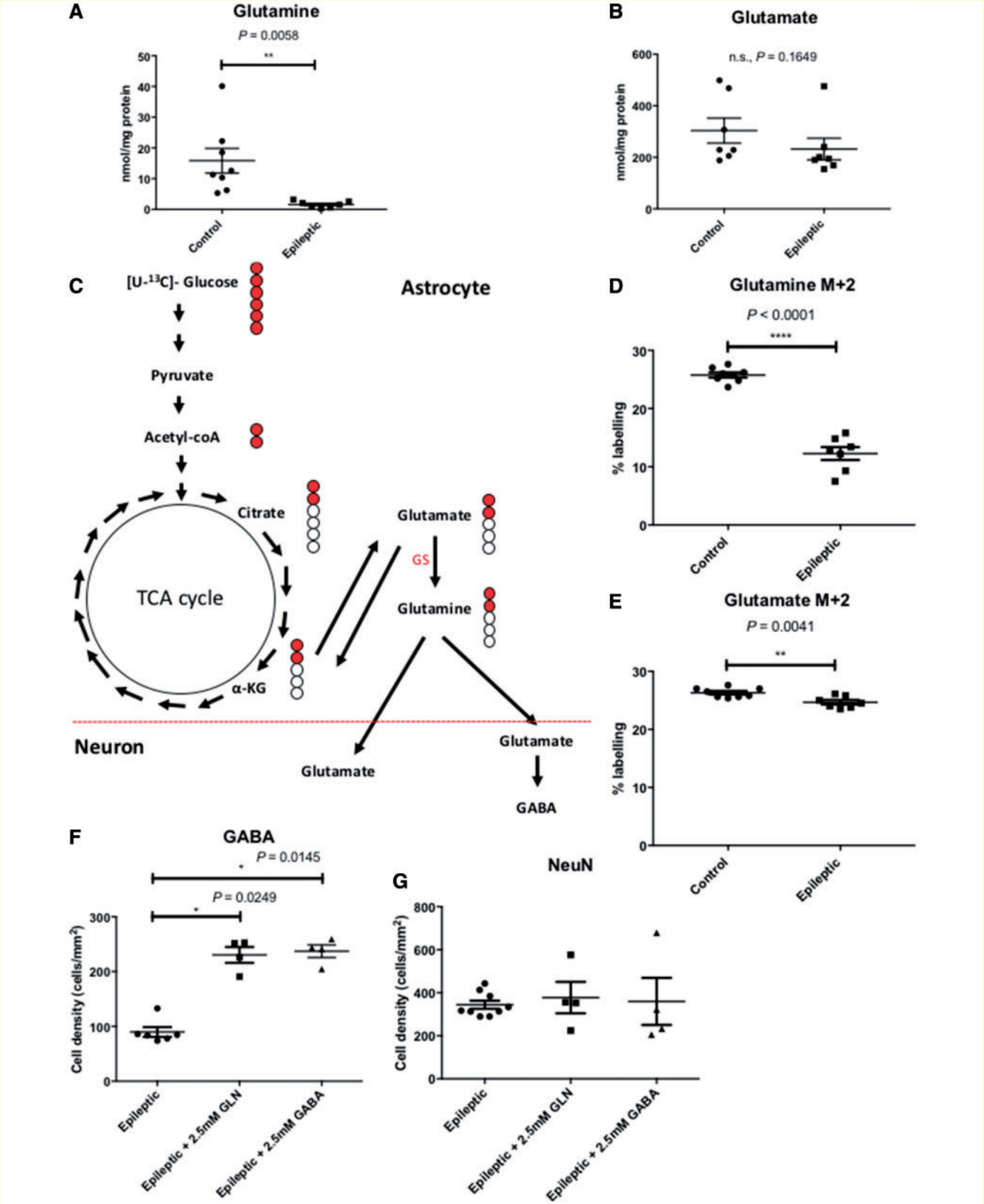

Figure 5 The downregulation of the astrocytic GABA-glutamate-glutamine cycle contributes to seizure generation *in vitro* via the intermediary molecule glutamine. There is a significant reduction in the tissue level of glutamine (n = 8 controls, n = 7 epileptic) (**A**), whilst tissue level of glutamate remains unaltered (n = 7 controls, n = 7 epileptic) (**B**). This reflects and confirms the pharmacological response of the epileptic tissue to glutamine but not glutamate. To examine the relative rate of the glutamate-glutamine cycle, we incubated the epileptic brain slices with [U-13C]-glucose to assess the incorporation of the ^{13}C-labelled atoms into the metabolites of the glutamate-glutamine cycle (**C**).

(continued)

of the downregulation of the astrocytic GABA-glutamate-glutamine cycle in mitochondrial epilepsy, we incubated hippocampal slices with uniformly labelled ^{13}C-glucose ([U-^{13}C]-glucose) and measured the incorporation of the labelled carbon atoms in various metabolic intermediates as glucose undergoes metabolic conversion (Fig. 5C). In astrocytes, after TCA cycle metabolism, the intermediary alpha-ketoglutarate can be converted to glutamate and can undergo further conversion to glutamine by the astrocyte-specific enzyme glutamine synthetase (Bak *et al.*, 2006; Anlauf and Derouiche, 2013). Glutamine is then released into the extracellular space as a precursor molecule for glutamate and GABA synthesis in excitatory and inhibitory neurons, respectively. Following initial TCA cycle metabolism, incorporation of the labelled carbon atoms into the GABA-glutamate-glutamine cycle is measured by the percentage of labelling in two of the carbon atoms (the M + 2 isotopomere) in the substrates glutamine and glutamate (Fig. 5C). We found a significant reduction in the M + 2 labelling of both glutamine (Fig. 5D) and glutamate (Fig. 5E) in the epileptic tissue; unsurprisingly the reduction being more pronounced in glutamine. Finally, to examine if there was an association between the GABA deficiency and the downregulation of the astrocytic GABA-glutamate-glutamine cycle, we examined the GABA expression in the neuronal population of the epileptic tissue following the rescue application of high concentrations (2.5 mM) of glutamine and GABA through immunohistochemistry. The cellular GABA expression was increased following the rescue application of GABA, but interestingly, also with the rescue application of glutamine (Fig. 5F). This upregulation of GABA expression was not accompanied by a concurrent increase in NeuN expression following any of the rescue applications, either with glutamine or GABA (Fig. 5G). These data suggest that instead of rescuing the loss of GABAergic cells, the application of glutamine and GABA act to increase GABA levels in the surviving neurons. Considering all these observations, the astrocytic GABA-glutamate-glutamine cycle appears to be downregulated in the epileptic tissue, which subsequently leads to deficiencies in the GABAergic system and the subsequent impairment of synaptic GABA release shifts the neuronal network towards seizure generation.

Glutamine synthetase deficiency in patient astrocytes could drive seizure generation in mitochondrial disease

The importance of the presence of fluorocitrate in this *in vitro* brain slice model of mitochondrial epilepsy for seizure generation suggests a critical pathogenic process mediated by the astrocytes. To date, this process remains unknown. Based on our data, we hypothesize that this pathogenic process could be the astrocytic GABA-glutamate-glutamine cycle, particularly the loss of the astrocyte-specific enzyme glutamine synthetase. To examine this, we measured glutamine levels in epileptic tissue following the rescue application of glutamine and GABA using HPLC. Measurements of glutamine levels in epileptic tissue revealed a significant increase following the rescue application of glutamine but no alteration in glutamine levels was observed with the rescue application of GABA (Fig. 6A). This scenario is only possible if the primary pathogenic process that leads to seizure generation is low astrocytic glutamine synthetase activity, an enzyme responsible for synthesis of glutamine from recycled glutamate or GABA (Bak *et al.*, 2006). Had this enzyme been functional, the supplementation of GABA would have led to the replenishment of tissue glutamine through this astrocytic enzyme. In light of this finding, we revisited the human neuropathological samples to examine glutamine synthetase expression within the astrocytes of the patients studied. Recent studies report the downregulation of glutamine synthetase in GFAP-positive astrocytes from patients with mesial TLE (Eid *et al.*, 2013); hence we also included sections of hippocampus from two TLE patients as a comparison. In healthy control samples, immunofluorescent labelling showed co-localization of glutamine synthetase and GFAP in astrocytes, whereas in samples from patients with mitochondrial epilepsy, glutamine synthetase was decreased within GFAP-positive astrocytes (Fig. 6B). An assessment of glutamine synthetase optical densities within GFAP-positive astrocytes revealed a significant reduction in expression in patients with TLE and patients with mitochondrial disease relative to controls (Fig. 6C). A significant reduction in the glutamine synthetase optical densities was observed within the GFAP-positive astrocytes of six of eight patients with mitochondrial disease; out of which five had recorded clinical

Figure 5 Continued

Briefly, [U-13C]-glucose enters the glutamate-glutamine cycle via the TCA cycle intermediate, α-ketoglutarate. Following the first turn of the TCA cycle, an incorporation of two of the ^{13}C-labelled atoms (M + 2) into the metabolites of the cycle, glutamate and glutamine, is expected. Measurement of the percentage of labelling of both M + 2 glutamine (**D**) and M + 2 glutamate (**E**) showed a significant reduction, confirming the downregulation of the astrocytic glutamate-glutamine cycle (n = 8 controls, n = 7 epileptic for both glutamine and glutamate M + 2). Finally, the application of glutamine onto the epileptic brain slices was able to increase GABA expression (**F**) in the surviving neurons without preventing neuronal loss or death (**G**) (n = 4 for epileptic + 2.5 mM glutamine and epileptic + 2.5 mM GABA). The epileptic group presented here as comparison were the data presented as the epileptic group in Fig. 2D and F. Together, this conclusively suggests the vital role that glutamine plays as an intermediary molecule of the astrocytic GABA-glutamate-glutamine cycle in seizure generation in this model of mitochondrial epilepsy. *$P \leqslant 0.05$, **$P \leqslant 0.01$, ***$P \leqslant 0.001$.

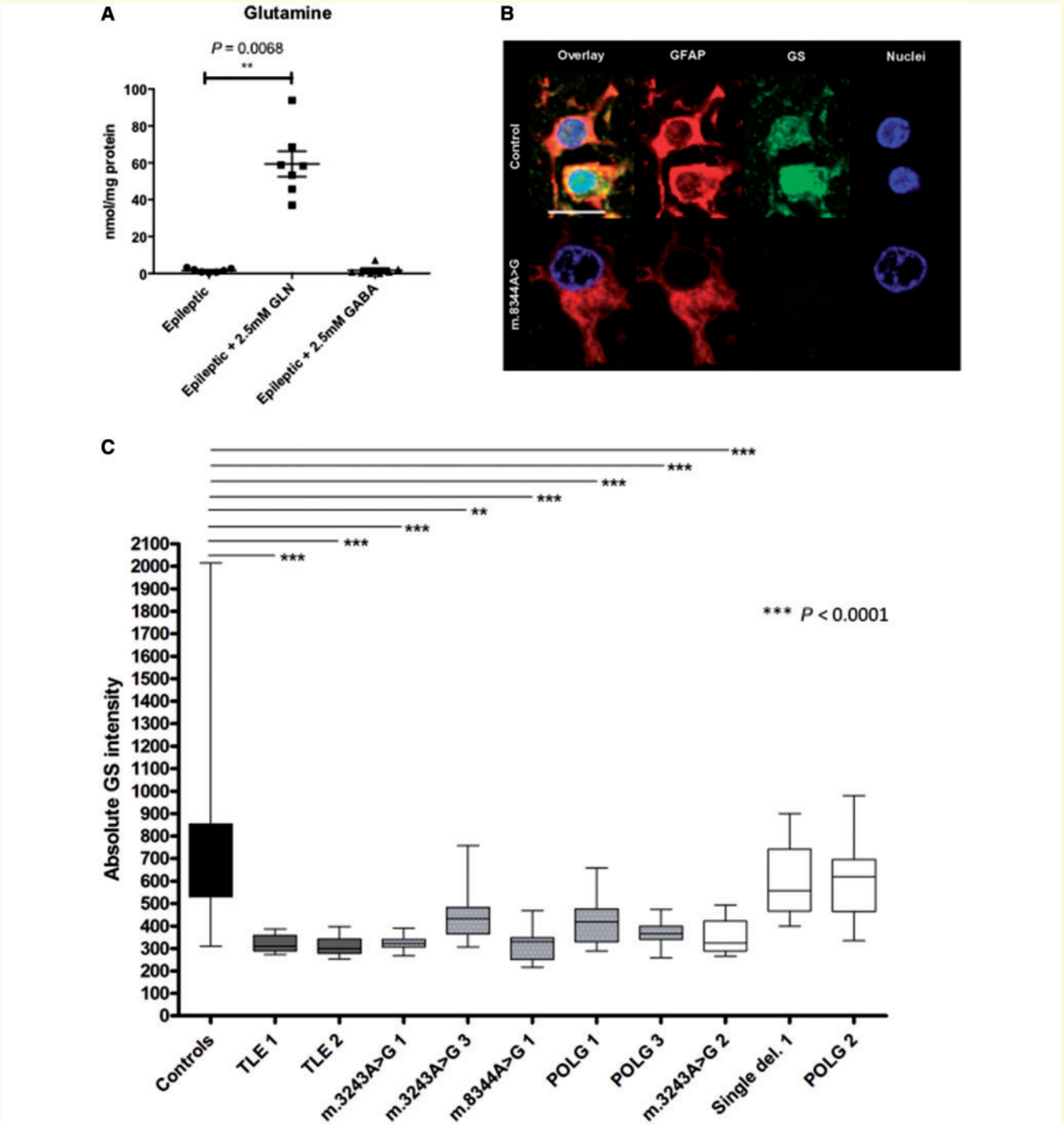

Figure 6 Glutamine synthetase activity is decreased in the epileptic rodent brain slices and concurrently, its expression is decreased in astrocytes in patients with mitochondrial epilepsy. Glutamine synthetase (GS) is an astrocytic-specific enzyme that synthesizes glutamine. Whilst the acute application of glutamine onto the epileptic tissue does unsurprisingly increase the tissue level of glutamine, it is striking that the application of equimolar GABA onto the epileptic tissue does not modify the tissue level of glutamine as compared to the epileptic tissue level (**A**) ($n = 7$ for epileptic + 2.5 mM glutamine and epileptic + 2.5 mM GABA). The epileptic group presented here as comparison were the data presented as the epileptic group in Fig. 5A. This suggests an underlying defect in the synthesis of glutamine, a process mediated by the astrocytic glutamine synthetase. This hypothesis was confirmed by observation in the post-mortem human brain tissue where control astrocytes show an abundance of glutamine synthetase within the astrocytes while patient astrocytes show a much lower level of glutamine synthetase (**B**). Scale bar = 10 μm. Quantification confirms significantly lower levels of glutamine synthetase in TLE (dark grey bars), patients with mitochondrial disease with epilepsy (grey bars with white dots), and patients with mitochondrial disease without epilepsy (white bars) as compared against control (black bar) (**C**). Interestingly, the glutamine synthetase level is also significantly lower in patients with mitochondrial disease with epilepsy compared to patients with mitochondrial disease without epilepsy. Data in **A** are presented as mean ± SEM and data in **C** are presented as box plots. *$P \leqslant 0.05$, ***$P \leqslant 0.001$.

history of epilepsy. One of the patients with significant reduction of glutamine synthetase optical density (Patient m.3243A>G 2) did not have a recorded history of epilepsy. The two patients with no history of epilepsy (Patients single deletion 1 and POLG 2) did not have a significant change in the glutamine synthetase optical density within the GFAP-positive astrocytes. This finding suggests that there is a trend towards the downregulation of glutamine synthetase expression being more prominent in the mitochondrial disease patient group, which had an epileptic phenotype as compared to those with no epileptic phenotype.

Discussion

In this study, we show distinct neuropathological changes in post-mortem sample of patients with mitochondrial epilepsy. Specifically, we demonstrate reactive astrogliosis and similar to previously reported findings in the neurons (Lax *et al.*, 2016), a loss of expression of mitochondrial complex I and more subtly, complex IV subunits in these reactive astrocytes. Based on these observations, we developed a novel functional *in vitro* brain slice model of mitochondrial epilepsy using pharmacological inhibition of mitochondrial complexes I and IV as well as specific inhibition of the astrocytic TCA cycle enzyme, aconitase. To our knowledge, this represents a unique *in vitro* model for mitochondrial epilepsy and we have demonstrated the face and predictive validity of the model. Furthermore, the model replicates the neuropathological observations reported in the patient samples that the *in vitro* model was derived from. We examined the role that astrocytes play in the generation of epileptiform discharges in this model and found crucial involvement of the astrocytic GABA-glutamate-glutamine cycle in the regulation of GABAergic mediated inhibition. In particular, glutamine emerges as a critical molecule mediating the interaction between the astrocytic and neuronal compartment in generating epileptiform network in this brain slice model of mitochondrial epilepsy. The depletion of tissue glutamine due to the loss of the astrocytic glutamine synthetase activity has been suggested to be an important pathogenic mechanism in epileptogenesis (Eid *et al.*, 2012). Inhibition of glutamine synthetase using methionine sulfoximine (MSO) has produced mixed results. In acute brain slices, preincubation with MSO alone was not able to produce epileptiform activity in rodent brain slices even in the presence of GABA receptor antagonists (which would disinhibit the slice) (Tani *et al.*, 2010). In a separate rodent cortical slice study, MSO induced an increase in glutamine levels, rather than a reduction, which would be expected from the inhibition of glutamine synthetase (Zielińska *et al.*, 2004). However, in direct contrast to the aforementioned *in vitro* work, the application of MSO *in vivo* has been shown to induce a decrease in the glutamine levels (Ghoddoussi *et al.*, 2010). Continuous microinfusion of MSO into the rodent hippocampus did lead to a deficiency in glutamine synthetase and the generation of recurrent seizures (Eid *et al.*, 2008), but there has been an argument proposed that the inhibition of glutamine synthetase by MSO is not directly related to the onset of seizures . Indeed MSO has a variety of additional pharmacological actions including inhibition of γ-glutamylcysteine synthetase (Richman *et al.*, 1973) and glutamate decarboxylase (Robertis *et al.*, 1967). Using an Emx1-IRES Cre mouse line, glutamine synthetase was selectively deleted in cortical and hippocampal structures and following a period of six or more weeks, these mice exhibited electrographic seizures (Zhou *et al.*, 2018). Interestingly, changes in neurochemistry, glia and neurovasculture preceded behavioural seizures suggesting that epileptic activity may not be directly related to glutamine synthetase deficiency but due to a consequence of a disease process involving gliosis and alterations in neurovascular coupling (Zhou *et al.*, 2018). Regardless, the wealth of literature does seem to suggest that at least *in vivo*, there is an association between glutamine synthetase inhibition and epileptic seizure. Reverting to our human neuropathological study, we discovered that in agreement with our *in vitro* model, a significant deficiency in glutamine synthetase expression was found in the astrocytes of the majority of the patients in our study with mitochondrial epilepsy as compared to healthy controls. Furthermore, patients with mitochondrial disease that do not exhibit epilepsy have a trend towards a better preserved glutamine synthetase expression as compared to those with mitochondrial epilepsy. This evidence supports a critical role for astrocytic dysfunction in determining whether patients with mitochondrial disease (who may have similar genetic mutation) present with an epileptic phenotype. This variation in phenotypic manifestation among patients with the same mitochondrial DNA mutation may be partly explained due to the heteroplasmic nature of mitochondrial DNA inheritance (Chinnery *et al.*, 2000) but as a whole, this phenotypic variation is a complex phenomenon that continues to be explored within the theme of mitochondrial genetics. In our model at the very least, glutamine and its associated metabolic pathway is emerging as a potentially important pathway in determining epileptic phenotype in patients with mitochondrial disease. Indeed, recent evidence has demonstrated that in response to mitochondrial DNA mutations, human cells rewire their glutamine metabolism depending on the severity of mitochondrial oxidative phosphorylation defect (Chen *et al.*, 2018). In this study, glutamine metabolism can sustain the cell metabolic requirement even under otherwise lethal oxidative inhibition (Chen *et al.*, 2018). This dependence of defective mitochondria on glutamine metabolism has previously also been shown in a mouse model of lung cancer (Strohecker *et al.*, 2013) and our result has further consolidated the importance of glutamine metabolism as a response to mitochondrial stress.

The results as outlined above emphasized the role that astrocyte metabolism plays in the generation of epilepsy. Indeed, a recent study has shown neurodegeneration upon

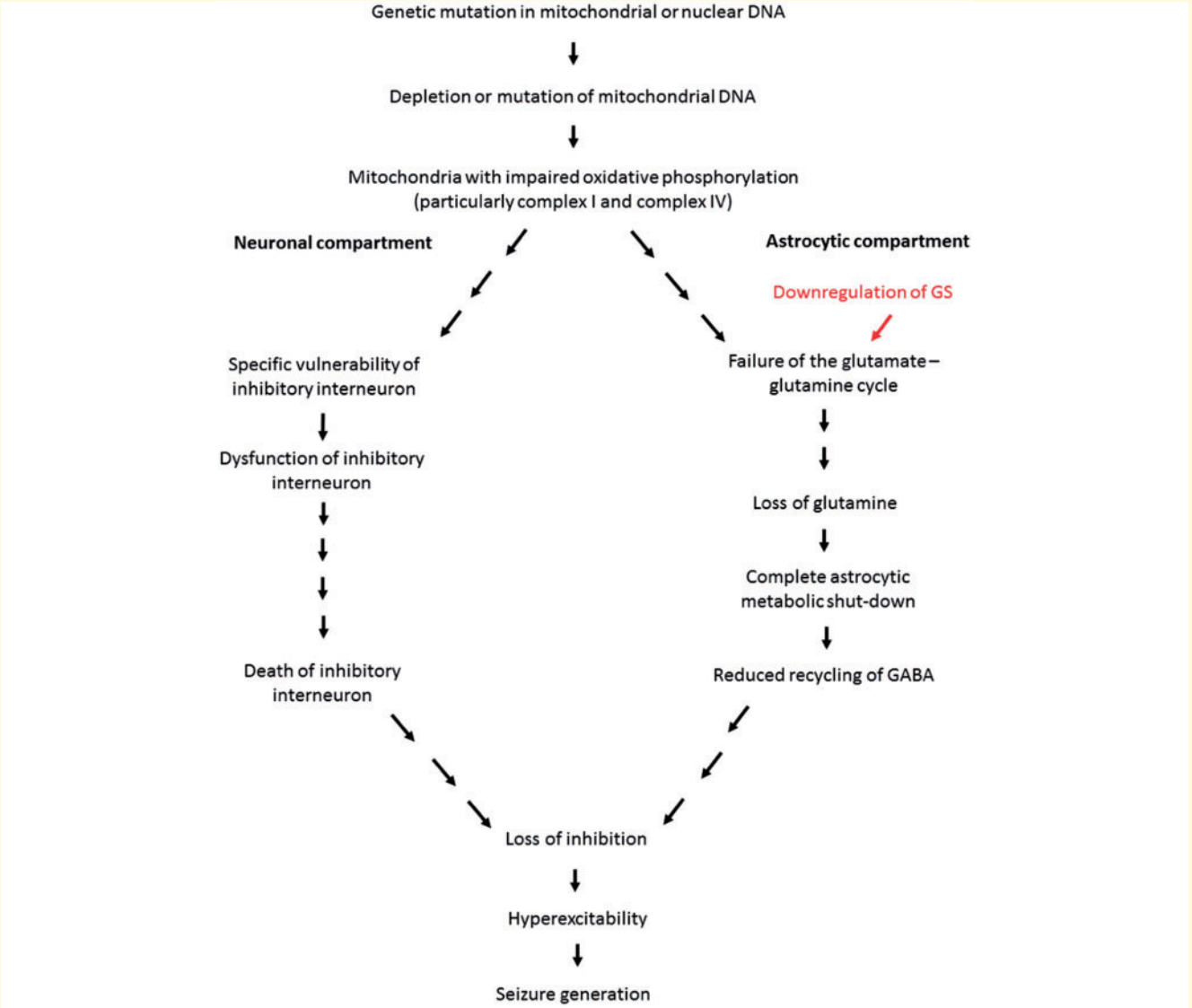

Figure 7 This model is proposed as a framework to understand the mechanisms behind seizure generation in mitochondrial epilepsy. We hereby propose the 'dual neuronal-astrocytic hit hypothesis' whereby we describe in detail the contribution and interdependence of both the neuronal and astrocytic compartment towards seizure generation in mitochondrial epilepsy based on data from our *in vitro* brain slice model. Mitochondrial disease begins with a genetic mutation in the mitochondrial or nuclear DNA, which leads to the depletion or mutation of mitochondrial DNA. This classically leads to the impairment of oxidative phosphorylation and in case of epilepsy, this is particularly in complexes I and IV. In neurons, due to the specific vulnerability of the inhibitory interneuron, this oxidative phosphorylation deficiency leads to the dysfunction and eventual death of the inhibitory interneurons. In the astrocytes, the impaired oxidative phosphorylation, importantly together with the downregulation of glutamine synthetase (GS), contributes towards the failure of the GABA-glutamate-glutamine cycle. This leads to a significant loss of glutamine, which leads to a complete astrocytic metabolic shutdown; hence a reduced recycling of GABA. Together, both the neuronal and astrocytic compartment dysfunction contributes towards an overall net loss of tissue inhibition. This generates a hyperexcitable network that eventually manifests as seizure generation. The downregulation of glutamine synthetase is highlighted in red as it seems to be an important determinant factor as to whether or not the patient will eventually manifest with an epileptic phenotype.

astrocyte-specific mitochondrial DNA depletion even though in this model, the animals were not reported to develop epilepsy (Ignatenko *et al.*, 2018). An interesting observation from this study is the vulnerability of the calbindin-interneuron towards the dysfunction of astrocyte metabolism brought about by the specific mitochondrial DNA depletion (Ignatenko *et al.*, 2018). This vulnerability of the interneuron is a phenomenon that is also observed in our model and thus strongly suggests the notion that for the development of epilepsy, the neuronal compartment must also be affected in addition to the astrocytic compartment. In particular, a significant loss of the inhibitory interneuron population will contribute to an overall loss of inhibitory tone in epilepsy associated with mitochondrial

disease (Lax *et al.*, 2016). This is expected as inhibitory interneurons have been reported to possess significant metabolic demand due to their firing pattern and activity (Gulyas *et al.*, 2006; Hazelton *et al.*, 2009; Kann *et al.*, 2011; Whittaker *et al.*, 2011). In this model, the loss of inhibitory interneuron population has been attributed to the respiratory chain inhibition, a process that has previously been associated with the dysfunction of the inhibitory interneurons (Kann *et al.*, 2011; Whittaker *et al.*, 2011; Lax *et al.*, 2016). Therefore, we propose the dual neuronal-astrocytic hypothesis as a framework for understanding the development of epilepsy in patients with mitochondrial disease (Fig. 7). This framework emphasizes the importance of the contribution from both the neuronal and astrocytic compartment towards creating a disinhibited neuronal network for seizure generation.

The novel *in vitro* brain slice model of mitochondrial epilepsy described in this study also enabled pharmacological assessment of mitochondrial epilepsy, in particular an examination of the efficacy of conventional antiepileptic agents. Although the assessment proves the super-refractory nature of the epileptiform discharges, it did demonstrate that barbiturates, at suprathreshold concentrations, may be the most effective agent to control mitochondrial epilepsy. More importantly, however, it seems that central to the seizure generation is the GABAergic system, particularly $GABA_A$ receptor modulation. As such, a number of potential therapeutic strategies emerge from this study. Firstly, targeting of the neuronal compartment by existing agents that modulate the $GABA_A$ receptor (e.g. using barbiturates as first-line monotherapy or benzodiazepines as an adjunct co-administered in conjunction with other agents that increase tissue GABA concentration), may provide symptomatic relief. Second, a more speculative therapeutic approach suggests that targeting of the astrocytic compartment by modulation of the GABA-glutamate-glutamine cycle to restore astrocytic control of the tissue inhibitory tone may prove beneficial. Oral supplementation of glutamine has been shown to increase GABA level in rodent's brain tissue (Wang *et al.*, 2007) and the use of glutamine supplementation as potential therapeutic approach is being studied in the context of ataxia-telangiectasia and Alzheimer's disease (Chen and Herrup, 2012; Chen *et al.*, 2016). At present, this is a novel therapeutic target for epilepsy and warrants further interrogation, which could yield an entirely novel class of antiepileptic agents.

This study contributes to the field of mitochondrial epilepsy but it also demonstrates features and findings that may be generalized to TLE and other epilepsy phenotypes. In our human neuropathology study, for instance, the deficiency in respiratory chain complexes I and IV as well as the deficiency in glutamine synthetase expression was observed in both patient groups of mitochondrial epilepsy and TLE. Therefore, while this model was initially developed for mitochondrial epilepsy, this suggests that the model may also be a model of TLE with a mitochondrial dysfunction component. Indeed, there have been reports of an association between mitochondrial dysfunction and TLE (Kunz *et al.*, 2000) as well as reports of mitochondrial dysfunction and metabolic changes in various animal models of epilepsy (Liang *et al.*, 2008; Kumar *et al.*, 2016; Gano *et al.*, 2018). The development of this model adds to the strong evidence that metabolic change and mitochondrial dysfunction could be an important pathogenic process in epileptogenesis. Whilst this brain slice model proves to be a robust and powerful model for understanding mitochondrial epilepsy, caution should be applied when interpreting these results in the context of human patients. Mitochondrial disease is undoubtedly a complex multisystem disease and the manifestation of seizures as a phenotype in each patient will depend on multiple contributing factors. Some of these have been described here, such as respiratory chain deficiency in both astrocytes and interneurons, the loss of inhibitory interneuron population, and the deficiency of astrocytic glutamine synthetase. The combination of all these factors will altogether determine if patients with a mitochondrial disease mutation will present with epilepsy in the clinic. Additionally, epilepsy is a progressive and evolving pathological condition. While results obtained from this study may characterize the early stage of the disease progression, it may not explain the evolution of the epileptic phenotype to the chronic condition at which point diagnosis is usually made in the patient. This indicates that findings from this study should be continued to an *in vivo* setting where such evolution of the phenotype can be explored. Furthermore, this model is not a genetic model of a specific syndrome of mitochondrial disease *per se*, rather it is a model of the phenotypic manifestation of mitochondrial disease, mitochondrial epilepsy, which may be present across multiple genotypes of mitochondrial disease. Therefore, results from this study should always be considered in the context of each of the specific syndromes within the mitochondrial disease diagnosis. Future studies may use these findings to generate a genetically modified animal model of mitochondrial epilepsy that is specific to each of the genotypes associated with mitochondrial epilepsy.

Acknowledgements

We thank M. Olahova, F. LeBeau, R. Lightowlers, M. Baker, and G. Gorman for helpful comments and discussions. We thank K. Newling for writing the Matlab script for the automated detection of the epileptiform discharges. We thank H. Thompson and A. Kosim for technical assistance with the biochemical experiments.

Funding

The study is primarily funded by the EPSRC Industrial CASE Award (EP/K50499X/1) studentship. This work was also supported by the following grants: The

Wellcome Centre for Mitochondrial Research (203105/Z/16/Z), The MRC Centre for Ageing and Vitality (MR/L016354/1), the UK NIHR Biomedical Research Centre in Age and Age Related Diseases award to the Newcastle upon Tyne Hospitals NHS Foundation Trust. We thank the Network of European Neuroscience Schools (NENS) Exchange Grant for funding the collaborative work done with University of Copenhagen.

Competing interests

The authors report no competing interests.

Supplementary material

Supplementary material is available at *Brain* online.

References

Anlauf E, Derouiche A. Glutamine synthetase as an astrocytic marker: its cell type and vesicle localization. Front Endocrinol 2013; 4: 144.

Bak LK, Schousboe A, Waagepetersen HS. The glutamate/GABA-glutamine cycle: aspects of transport, neurotransmitter homeostasis and ammonia transfer. J Neurochem 2006; 98: 641–53.

Bindoff LA, Engelsen BA. Mitochondrial diseases and epilepsy. Epilepsia 2012; 53: 92–7.

Chan F, Lax NZ, Davies CH, Turnbull DM, Cunningham MO. Neuronal oscillations: a physiological correlate for targeting mitochondrial dysfunction in neurodegenerative diseases? Neuropharmacology 2016; 102: 48–58.

Chen J, Chen Y, Vail G, Chow H, Zhang Y, Louie L, et al. The impact of glutamine supplementation on the symptoms of ataxia-telangiectasia: a preclinical assessment. Mol Neurodegener 2016; 11: 60.

Chen J, Herrup K. Glutamine acts as a neuroprotectant against DNA damage, beta-amyloid and H2O2-induced stress. PLOS ONE 2012; 7: e33177.

Chen Q, Kirk K, Shurubor YI, Zhao D, Arreguin AJ, Shahi I, et al. Rewiring of glutamine metabolism is a bioenergetic adaptation of human cells with mitochondrial DNA mutations. Cell Metabol 2018; 27: 1007–25.e5.

Chevallier JA, Von Allmen GK, Koenig MK. Seizure semiology and EEG findings in mitochondrial diseases. Epilepsia 2014; 55: 707–12.

Chinnery PF, Thorburn DR, Samuels DC, White SL, Dahl HM, Turnbull DM, et al. The inheritance of mitochondrial DNA heteroplasmy: random drift, selection or both? Trends Genet: TIG 2000; 16: 500–5.

Chrysostomou A, Grady JP, Laude A, Taylor RW, Turnbull DM, Lax NZ. Investigating complex I deficiency in Purkinje cells and synapses in patients with mitochondrial disease. Neuropathol Appl Neurobiol 2015; 42: 477–92.

Cunningham MO, Roopun A, Schofield IS, Whittaker RG, Duncan R, Russell A, et al. Glissandi: transient fast electrocorticographic oscillations of steadily increasing frequency, explained by temporally increasing gap junction conductance. Epilepsia 2012; 53: 1205–14.

Eid T, Behar K, Dhaher R, Bumanglag AV, Lee T-SW. Roles of glutamine synthetase inhibition in epilepsy. Neurochem Res 2012; 37: 2339–50.

Eid T, Ghosh A, Wang Y, Beckström H, Zaveri HP, Lee T-SW, et al. Recurrent seizures and brain pathology after inhibition of glutamine synthetase in the hippocampus in rats. Brain 2008; 131: 2061–70.

Eid T, Lee TSW, Wang Y, Peréz E, Drummond J, Lauritzen F, et al. Gene expression of glutamate metabolizing enzymes in the hippocampal formation in human temporal lobe epilepsy. Epilepsia 2013; 54: 228–38.

Finsterer J, Mahjoub SZ. Presentation of adult mitochondrial epilepsy. Seizure 2013; 22: 119–23.

Fonnum F, Johnsen A, Hassel B. Use of fluorocitrate and fluoroacetate in the study of brain metabolism. Glia 1997; 21: 106–13.

Gano LB, Liang L-P, Ryan K, Michel CR, Gomez J, Vassilopoulos A, et al. Altered mitochondrial acetylation profiles in a kainic acid model of temporal lobe epilepsy. Free Rad Biol Med 2018; 123: 116–24.

Ghoddoussi F, Galloway MP, Jambekar A, Bame M, Needleman R, Brusilow WSA. Methionine sulfoximine, an inhibitor of glutamine synthetase, lowers brain glutamine and glutamate in a mouse model of ALS. J Neurolog Sci 2010; 290: 41–7.

Gorman GS, Schaefer AM, Ng Y, Gomez N, Blakely EL, Alston CL, et al. Prevalence of nuclear and mitochondrial DNA mutations related to adult mitochondrial disease. Ann Neurol 2015; 77: 753–9.

Greenfield LJ. Molecular mechanisms of antiseizure drug activity at GABA(A) receptors. Seizure 2013; 22: 589–600.

Gulyas AI, Buzsaki G, Freund TF, Hirase H. Populations of hippocampal inhibitory neurons express different levels of cytochrome c. Eur J Neurosci 2006; 23: 2581–94.

Gusel'nikova VV, Korzhevskiy DE. NeuN as a neuronal nuclear antigen and neuron differentiation marker. Acta Naturae 2015; 7: 42–7.

Hassel B, Paulsen RE, Johnsen A, Fonnum F. Selective inhibition of glial cell metabolism in vivo by fluorocitrate. Brain Res 1992; 576: 120–4.

Hazelton JL, Petrasheuskaya M, Fiskum G, Kristian T. Cyclophilin D is expressed predominantly in mitochondria of gamma-aminobutyric acidergic interneurons. J Neurosci Res 2009; 87: 1250–9.

Ignatenko O, Chilov D, Paetau I, de Miguel E, Jackson CB, Capin G, et al. Loss of mtDNA activates astrocytes and leads to spongiotic encephalopathy. Nature Commun 2018; 9: 70.

Kann O, Huchzermeyer C, Kovács R, Wirtz S, Schuelke M. Gamma oscillations in the hippocampus require high complex I gene expression and strong functional performance of mitochondria. Brain 2011; 134: 345–58.

Khurana DS, Salganicoff L, Melvin JJ, Hobdell EF, Valencia I, Hardison HH, et al. Epilepsy and respiratory chain defects in children with mitochondrial encephalopathies. Neuropediatrics 2008; 39: 8–13.

Kumar MG, Rowley S, Fulton R, Dinday MT, Baraban SC, Patel M. Altered glycolysis and mitochondrial respiration in a zebrafish model of dravet syndrome. eNeuro 2016; 3. doi: 10.1523/ENEURO.0008-16.2016.

Kunz WS, Kudin AP, Vielhaber S, Blümcke I, Zuschratter W, Schramm J, et al. Mitochondrial complex I deficiency in the epileptic focus of patients with temporal lobe epilepsy. Ann Neurol 2000; 48: 766–73.

Lax NZ, Campbell GR, Reeve AK, Ohno N, Zambonin J, Blakely E, et al. Loss of myelin-associated glycoprotein in kearns-sayre syndrome. Arch Neurol 2012a; 69: 490–9.

Lax NZ, Grady J, Laude A, Chan F, Hepplewhite PD, Gorman G, et al. Extensive respiratory chain defects in inhibitory interneurones in patients with mitochondrial disease. Neuropathol Appl Neurobiol 2015; 42: 180–93.

Lax NZ, Grady J, Laude A, Chan F, Hepplewhite PD, Gorman G, et al. Extensive respiratory chain defects in inhibitory interneurones in patients with mitochondrial disease. Neuropathol Appl Neurobiol 2016; 42: 180–93.

Lax NZ, Hepplewhite PD, Reeve AK, Nesbitt V, Mcfarland R, Jaros E, et al. Cerebellar ataxia in patients with mitochondrial DNA disease. J Neuropathol Exp Neurol 2012b; 71: 148–61.

Lax NZ, Pienaar IS, Reeve AK, Hepplewhite PD, Jaros E, Taylor RW, et al. Microangiopathy in the cerebellum of patients with mitochondrial DNA disease. Brain 2012c; 135: 1736–50.

Lax NZ, Whittaker RG, Hepplewhite PD, Reeve AK, Blakely EL, Jaros E, et al. Sensory neuronopathy in patients harbouring recessive polymerase γ mutations. Brain 2011; 135: 62–71.

Liang L-P, Jarrett SG, Patel M. Chelation of mitochondrial iron prevents seizure-induced mitochondrial dysfunction and neuronal injury. J Neurosci 2008; 28: 11550–6.

McNair LF, Kornfelt R, Walls AB, Andersen JV, Aldana BI, Nissen JD, et al. Metabolic characterization of acutely isolated hippocampal and cerebral cortical slices using [U-(13)C]Glucose and [1, 2-(13)C]Acetate as substrates. Neurochem Res 2017; 42: 810–26.

Ng YS, Grady JP, Lax NZ, Bourke JP, Alston CL, Hardy SA, et al. Sudden adult death syndrome in m.3243A > G-related mitochondrial disease: an unrecognized clinical entity in young, asymptomatic adults. Eur Heart J 2015; 37: 2552–9.

Reeve A, Meagher M, Lax N, Simcox E, Hepplewhite P, Jaros E, et al. The impact of pathogenic mitochondrial DNA mutations on substantia nigra neurons. J Neurosci 2013; 33: 10790–801.

Rho JM, Donevan SD, Rogawski MA. Direct activation of GABAA receptors by barbiturates in cultured rat hippocampal neurons. J Physiol 1996; 497(Pt 2): 509–22.

Richman PG, Orlowski M, Meister A. Inhibition of γ-Glutamylcysteine Synthetase by l-Methionine-S-sulfoximine. J Biol Chem 1973; 248: 6684–90.

Robertis E, Sellinger OZ, Rodríuez de Lores Arnaiz G, Alberici M, Zieher LM. Nerve endings in methionine sulphoximine convulsant rats, a neurochemical and ultrastructural study*. J Neurochem 1967; 14: 81–9.

Roopun AK, Simonotto JD, Pierce ML, Jenkins A, Nicholson C, Schofield IS, et al. A nonsynaptic mechanism underlying interictal discharges in human epileptic neocortex. Proc Natl Acad Sci USA 2010; 107: 338–43.

Simon A, Traub RD, Vladimirov N, Jenkins A, Nicholson C, Whittaker RG, et al. Gap junction networks can generate both ripple-like and fast ripple-like oscillations. Eur J Neurosci 2014; 39: 46–60.

Sofroniew MV. Molecular dissection of reactive astrogliosis and glial scar formation. Trends Neurosci 2009; 32: 638–47.

Strohecker AM, Guo JY, Karsli-Uzunbas G, Price SM, Chen GJ, Mathew R, et al. Autophagy sustains mitochondrial glutamine metabolism and growth of BrafV600E-driven lung tumors. Cancer Discov 2013; 3: 1272–85.

Swanson RA, Graham SH. Fluorocitrate and fluoroacetate effects on astrocyte metabolism in vitro. Brain Res 1994; 664: 94–100.

Tani H, Dulla CG, Huguenard JR, Reimer RJ. Glutamine is required for persistent epileptiform activity in the disinhibited neocortical brain slice. J Neurosci 2010; 30: 1288–300.

Wang L, Maher TJ, Wurtman RJ. Oral l-glutamine increases GABA levels in striatal tissue and extracellular fluid. FASEB J 2007; 21: 1227–32.

Whittaker RG, Devine HE, Gorman GS, Schaefer AM, Horvath R, Ng Y, et al. Epilepsy in adults with mitochondrial disease: a cohort study. Ann Neurol 2015; 78: 949–57.

Whittaker RG, Turnbull DM, Whittington MA, Cunningham MO. Impaired mitochondrial function abolishes gamma oscillations in the hippocampus through an effect on fast-spiking interneurons. Brain 2011; 134: e180–e.

Zhou Y, Dhaher R, Parent M, Hu Q-X, Hassel B, Yee S-P, et al. Selective deletion of glutamine synthetase in the mouse cerebral cortex induces glial dysfunction and vascular impairment that precede epilepsy and neurodegeneration. Neurochem Int 2018. doi: 10.1016/j.neuint.2018.07.009.

Zielińska M, Stafiej A, Law RO, Albrecht J. Effects of methionine sulfoximine on the glutamine and glutamate content and cell volume in rat cerebral cortical slices: involvement of mechanisms not related to inhibition of glutamine synthesis. NeuroToxicology 2004; 25: 443–9.